Fluctuations of DNA mobility in nanofluidic entropic traps

Lingling Wu[1] and Stephen Levy[1,2,a)]
[1]*Department of Materials Science and Engineering, Binghamton University, Binghamton, New York 13902, USA*
[2]*Department of Physics, Binghamton University, Binghamton, New York 13902, USA*

(Received 30 May 2014; accepted 25 June 2014; published online 8 July 2014)

We studied the mobility of DNA molecules driven by an electric field through a nanofluidic device containing a periodic array of deep and shallow regions termed entropic traps. The mobility of a group of DNA molecules was measured by fluorescent video microscopy. Since the depth of a shallow region is smaller than the DNA equilibrium size, DNA molecules are trapped for a characteristic time and must compress themselves to traverse the boundary between deep and shallow regions. Consistent with previous experimental results, we observed a nonlinear relationship between the mobility and electric field strength, and that longer DNA molecules have larger mobility. In repeated measurements under seemingly identical conditions, we measured fluctuations in the mobility significantly larger than expected from statistical variation. The variation was more pronounced for lower electric field strengths where the trapping time is considerable relative to the drift time. To determine the origin of these fluctuations, we investigated the dependence of the mobility on several variables: DNA concentration, ionic strength of the solvent, fluorescent dye staining ratio, electroosmotic flow, and electric field strength. The mobility fluctuations were moderately enhanced in conditions of reduced ionic strength and electroosmotic flow. © *2014 AIP Publishing LLC*. [http://dx.doi.org/10.1063/1.4887395]

I. INTRODUCTION

The separation of DNA molecules of different length and topology is an integral process for many sectors of biological science and in pharmaceutical industry. Micro and nanofluidic instruments offer a compelling alternative to gels for the separation of nucleic acids because of the precision in their fabrication.[1] Fluidic structures can be made in a variety of length scales relevant to the nucleic acid of interest, spanning decades from tens of nanometers to tens of microns, and their periodicity can likewise be controlled with high precision.[2] Nanofluidic technology has improved our understanding of the physical mechanisms useful in separating polyelectrolytes.[3]

The separation of long DNA molecules using microfabricated arrays of repeating deep and shallow wells, termed entropic traps, was pioneered by Han and Craighead.[4–7] A DNA molecule with a radius of gyration larger than the shallow depth will compress in order to traverse the boundary between a deep and shallow region when driven by a large enough external potential. Such a potential overcomes the increase in entropy due to the reduced molecular configurations available when compressed, allowing the molecule to reduce its free energy. Han and Craighead developed a model for the DNA mobility based on the free energy difference between the deep and shallow regions.[7] In this model, the trapping time τ when a molecule is stalled at a boundary between a deep and shallow region is given by

$$\tau = \tau_0 \exp(\alpha / E_s kT), \tag{1}$$

a)Author to whom correspondence should be addressed. Electronic mail: slevy@binghamton.edu.

where τ_0 is pre-factor that depends inversely on the DNA length, α is a constant, E_s is the electric field in the shallow region, and kT is the thermal energy. Based on their experimental results, they surmised that the pre-factor decreases with length since a larger molecule presents more cross sectional area to the shallow slit entrance and can effectively make more attempts per unit time to overcome the energy barrier. They demonstrated that the energy barrier was length independent.

There have been several theoretical investigations and simulations employed to explain the length dependent translocation of a free energy barrier by a polymer. Though questions still persist about some key elements of the process, the main finding that the length dependent mobility results from the pre-factor τ_0 has been validated. Using a bond fluctuation Monte Carlo simulation, Tessier and Slater[8] observed a length dependent polymer mobility that agreed with the free energy model of Han and Craighead.[7] They added that an important factor in explaining the length dependent trapping time results from the compression of a molecule at the entrance to the shallow slit due to the stronger region of the electric field. Sakaue[9] also stressed the importance of polymer deformation in explaining the length dependent results. Panwar and Kumar[10] used a Brownian dynamic simulation that verified some theoretical predictions of Sebastian and Paul;[11] namely, that τ_0 scales inversely with length for polymers that traverse the barrier in a hairpin configuration and that τ_0 is independent of length for polymers that traverse linearly. Wong and Muthukumar[12] devised a theory showing that τ_0 decreased with length for hairpins (with a power of $\sim$0.4) but that it increased with length for linear configurations. The experimental results of Han and Craighead are explained then by the much high probability of hairpin traversal for the length of DNA molecules used. Other simulations have yielded similar results to those observed experimentally[13,14] with minor variations on the length dependent mechanism.[15] None of the simulations has included hydrodynamic interactions or electroosmotic flow.[8,10,14,15]

We are motivated to further investigate the entropic trapping mechanism to probe some of these elements that are still not clearly understood. Single molecule experiments can shed light on the role of the electric field deformation at the entrance to the shallow region and on the trapping time probability function. Predictions of polymer separation based on topology[8,14] from simulations have not been experimentally verified and could corroborate the dependence of τ_0 on polymer size. Tessier and Slater[16] have proposed a separation mechanism based on an asymmetric time varying electric field whereby molecules longer than a cutoff length move backward through an entropic array and shorter molecules move forward. In fact, Thomas *et al.*[17] have successfully implemented this mode of separation in a periodic array of deep and shallow regions using molecules with sizes smaller than the shallow depth. The basis of DNA separation in their device results from a length based difference in partition coefficients and is physically distinct from the entropic trapping mechanism studied herein. We shall elaborate on an interesting result of their experiment in Sec. III C.

Before addressing these intriguing aspects of the entropic trapping mechanism, we sought to calibrate our measurements by comparison with previous results. While our calibrations were reasonably validated as will be detailed, we observed fluctuations in DNA mobility, which were larger than expected from statistical variation. The fluctuations occurred in repetitions of seemingly identical experimental trials. Consequently, our original aim was diverted toward examining these fluctuations so that we could reduce them or at least quantify the time scale over which they were significant. We were partially successful.

II. PROCEDURE

A. Fabrication

Entropic trap devices were made by a two-step photolithography process using a 500 μm thick fused silica wafer (Mark Optics) as a substrate. The patterned silica was removed in a reactive ion etch chamber (Oxford, Plasmalab 80 Plus) using a combination of CF_4 and O_2 gases for the first (shallow) layer and a combination of CHF_3 and O_2 gases for the aligned second (deep) layer. Alignment was performed manually using a contact lithography tool. Loading

holes were punched through the fused silica wafer using a micro-abrasive blaster to provide a fluid connection to the devices. The wafer was cleaned thoroughly in Remover PG (MicroChem), acetone, isopropyl alcohol, Nano-Strip (Cyantek), and deionized (DI) water baths. The etched wafer and a 170 μm thick fused silica cover wafer (Mark Optics) were cleaned separately with a 1:1:5 solution of ammonium hydroxide, hydrogen peroxide, and DI water at 75 °C for 10 min. The two wafers were touch-bonded and annealed in a high temperature furnace at 1050 °C (above the glass transition temperature of fused silica) for several hours. Pipette tips were cut with a razor blade and attached with silicon adhesive (Dow Corning, 732) to create fluidic reservoirs of approximately 50 μl.

There are typically sixteen individual entropic trap devices fabricated on each wafer. A given device has the shape of a *T,* consisting of a loading channel, a separation channel, and three reservoirs (left, right, and loading) as shown in Fig. 1. The loading channel intersects the separation channel at the entrance to an array of 1200 entropic traps. A given trap has a deep and shallow region each with a length (in the direction of DNA flow) of 6 μm, and thus a period L_p of 12 μm. The depth of the shallow region, d_s, was measured to be 63 ± 5 nm (mean $\pm$ standard deviation) by a surface profilometer (Veeco, Dektak 150) with sub-nanometer resolution. The depth of the deep region, d_d, was found to be 1455 ± 50 nm. The widths of the shallow and deep regions are 30 and 33 μm, respectively, allowing for overlap in case of slight misalignment. The length of the separation channel is approximately 2 cm.

B. DNA preparation and experimental protocol

10 kbp DNA (New England Biolabs), λ DNA (New England Biolabs, 48.502 kbp), and T4 DNA (Wako Nippon Gene, 165.6 kbp) were used in our experiments. These DNA samples were diluted to 1% of their respective stock concentration (0.32 μg/μl for T4 DNA; 0.5 μg/μl for λ DNA; and 0.5 μg/μl for 10 kbp DNA) and stained with YOYO1-iodide (Invitrogen) for visualization under fluorescent light. The nominal experiments were performed with a staining ratio of 5 DNA base pairs per 1 YOYO-1 molecule (5:1); in additional experiments the staining was reduced to a ratio of 20:1. Tris, Borate, and EDTA (Sigma-Aldrich) were mixed with deionized water to make a Tris-borate-EDTA (TBE) buffer at a pH of 8.2, as measured by a pH probe (Symphony, VWR). The buffer was filtered (Whatman, Anotop 10, 0.02 μm) prior to use. The nominal experiments were conducted using a 5× concentration of TBE (445 mM Tris-Borate, 10 mM of EDTA); in additional experiments the concentration was reduced to 3×. The TBE buffers were mixed with 3% (by volume) of β-mercaptoethanol to reduce photobleaching. The ionic strength is defined as $I = 1/2\sum_i c_i z_i^2$, where c_i and z_i are the molar concentration and charge of the ith ion, respectively. The 5× and 3× buffers contain an ionic strength of approximately 160 and 95 mM, respectively, as determined from the pK_b value of Tris base and the respective pK_a values of boric acid and the polyprotic acids of EDTA (the effects of β-mercaptoethanol on the ionic strength and pH are less than 1% at these ionic strengths). In some experiments we added 2% poly(*n*-vinylpyrrolidone) (PVP, Sigma-Aldrich, molecular mass 10 000 g/mol) to the TBE buffer to reduce the electro-osmotic flow. For all fluid manipulations involving DNA, we used pipette tips that were manually cut approximately 1 cm from the bottom to reduce unwanted DNA fractionation.

An electric field was generated by a dc power supply connected to gold wires that were inserted into the reservoirs as electrodes. An inverted optical microscope (Olympus IX71) with a 60×, 1.3 NA oil immersion objective lens (Olympus), a mercury arc-lamp excitation (EXFO, X-cite 120 pc), and an appropriate spectral filter set (Semrock, 3035) were used to observe the DNA. Images were recorded with an electron multiplying charge-coupled device camera (Photometrics, Evolve 512) using Labview (National Instruments) custom software. The ionic current was measured with a current amplifier (Keithley, 427) in series with the power supply using custom Labview software.

In typical DNA electrophoresis separation experiments, it is necessary to form a spatially concentrated region of DNA, referred to here as a plug, prior to sending the DNA through the separation channel to achieve maximal resolution. We describe the protocol for forming the

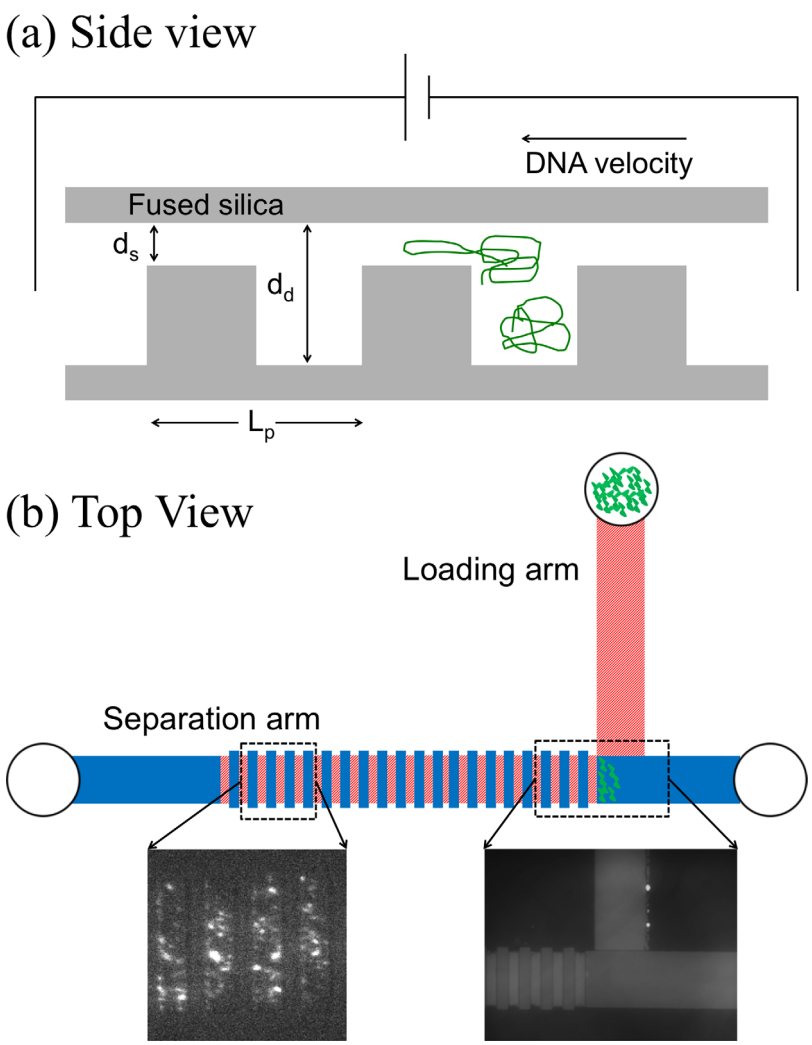

FIG. 1. Schematic illustration of an entropic trap device etched in fused silica shown from side (a) and top (b) views, not to scale. (a) DNA molecules travel opposite to the electric field and must deform to cross from a deep to shallow area. The ratio of deep to shallow regions is approximately 23. (b) An experiment is performed by first concentrating DNA molecules at the entrance to the separation channel (green wiggles) and subsequently running them through the separation channel using an applied electric field. The right inset of (b) is a bright field micrograph of the trapping region at the beginning of the separation channel. The left inset of (b) is a fluorescent micrograph of T4 DNA molecules moving across entropic traps. The width of the channel, vertical size of the separation channel that is perpendicular to the DNA migration direction, is approximately 30 μm. The deep regions (solid blue) within the separation channel are 10% wider than the shallow regions (red hash).

plug and measuring the DNA mobility in this paragraph, which we denote as a trial. An experiment is meant to indicate a series of trials (typically 4) run under identical conditions. Immediately before running an experiment, the device was filled with the buffer solution and a voltage was applied between the left and right reservoirs for 30 min in order to equilibrate the buffer. A DNA solution in the same buffer was pipetted into the loading reservoir and driven into the separation channel by an applied voltage between the loading and right reservoir. By applying a relatively low voltage ($\sim$5 V) between the separation channel reservoirs, we concentrated a plug of DNA at the beginning of the separation channel trap region. The voltage was experimentally tuned to be below the value that would cause the DNA to deform and cross the traps. We set the camera a known distance L from the entrance of the entropic traps using a calibrated stage controller (Prior PS3J100). The voltage applied to form the plug of DNA was turned off for tens of seconds to allow the DNA to equilibrate spatially along the channel width

dimension. We then applied a voltage across the separation channel reservoirs, to drive the DNA through the entropic trap array, and simultaneously started recording images at approximately 5 frames per second. We note that the DNA in all experiments moved in the direction opposite to the electric field, as a negatively charged object would. This is in contrast to capillary electrophoresis where the electroosmotic flow caused by the negatively charged capillary often dominates and the DNA is dragged in the electric field direction.

We used custom software written in MATLAB (The MathWorks) to analyze the images. Each image was background subtracted based on the fluorescent intensity outside of the fluidic channel region. We measured the average intensity per pixel in each frame in a user-selected region of interest that typically encompassed the channel width and several deep and shallow periods. We smoothed the intensity as a function of time using a moving average with a sliding window of 50 frames (10 s) as shown in Fig. 2(a). The smoothed intensity as a function of time is typically Gaussian. We identified the connected portion of the smoothed intensity that is three standard deviations above the background level, as measured from the first 20% of the smoothed intensity. This portion is used to calculate the intensity weighted mean arrival time T of the DNA, after they have moved a distance L, and the standard deviation of the arrival time δT. These values are insensitive to the size of the selected region of interest.

For a given voltage applied across the separation channel, we inferred the electric field in the deep and shallow regions using the measured channel dimensions. The resistivity of any portion of the separation channel is assumed to be proportional to the channel length (direction along the channel) and inversely proportional to the cross-sectional area. By combining the resistivity of the deep and shallow regions in series we find that more than 90% of the applied voltage is dropped across the shallow regions. The ratio of the electric field in the deep and shallow regions is approximately equal to the ratio of the deep and shallow channel depths; there is a small difference due to the channel segments connecting the left and right reservoirs to the entropic trap array. We measure the mobility as a function of the average electric field, given by $E_{av} = (E_s + E_d)/2 = E_s(1+\gamma)/(2\gamma)$, where E_s and E_d are the electric fields in the shallow and deep regions, respectively, and γ is the ratio of the deep to shallow depths. Based on the measured channel dimensions $\gamma = 23 \pm 2$.

C. Model

Following the analysis of Han and Craighead,[7] we expect that the time-averaged mobility should be given by

$$\mu = \mu_0 \frac{t}{t+\tau}, \tag{2}$$

where μ_0 is the free solution mobility, t is the time to traverse the shallow and deep regions (ignoring the entropic trap), and τ is the time spent at the entrance to an entropic trap, referred to as the trapping time. We have assumed that the free solution mobility is independent of the channel depth, which we will return to in Sec. III A. The mobility expression reduces to the free solution mobility in the limit that the trapping time is negligible. Note that the trapping time is distinct from the crossing, or transit time, that is typically measured in nanopore experiments by the duration of a current blockade. The time to traverse a shallow and deep region (ignoring the trapping time) is given by

$$t = \frac{L_p}{2\mu_0}\left(\frac{1}{E_s} + \frac{1}{E_d}\right) = \frac{L_p}{\mu_0 E_{av}} \frac{(1+\gamma)^2}{4\gamma}, \tag{3}$$

which when substituted into Eq. (2) leads to an expected mobility of

$$\mu = \frac{L_p}{(t+\tau)E_{av}} \frac{(1+\gamma)^2}{4\gamma}. \tag{4}$$

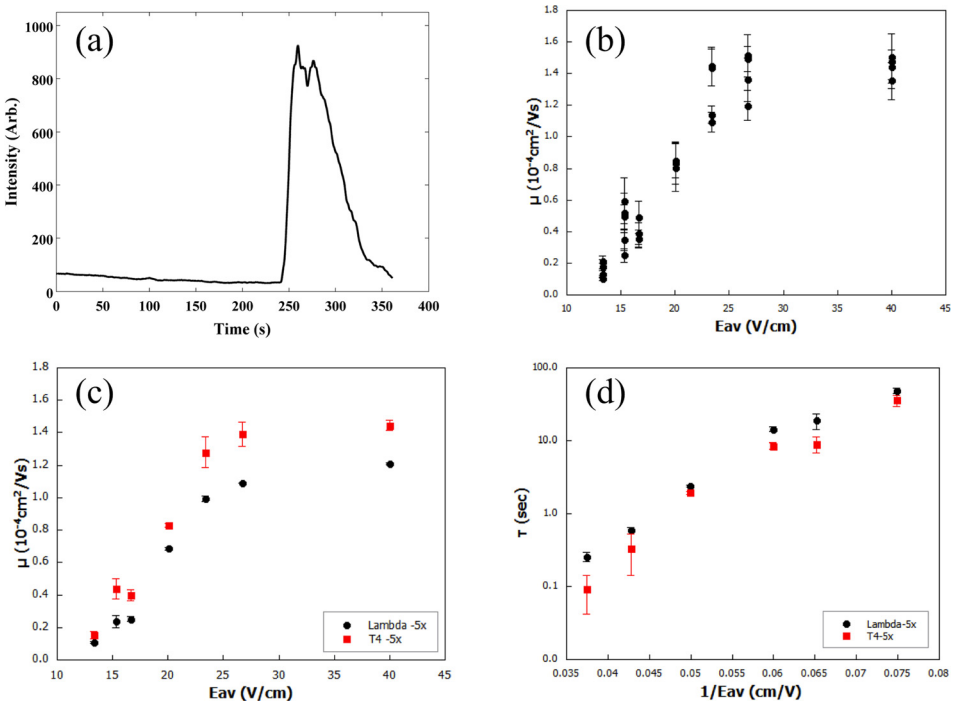

FIG. 2. (a) Fluorescent intensity of T4 DNA molecules at a fixed location a few millimeters downstream from the entrance to the separation channel driven by a 40 V/cm average electric field as a function of time. The intensity is summed over a region of interest, background corrected, and smoothed using a sliding window. (b) Mobility of T4–5x DNA as a function of the average electric field. Each data point represents one trial and the error bar represents the uncertainty propagated from the width of the time peak shown in (a). (c) Average mobility as a function of the average electric field for T4–5x (red square) and lambda–5x (black circle) DNA. The points represent the mobility averaged over four trials and the error bars represent the standard error of the mean. (d) Trapping lifetime (τ) of T4–5x (red square) and lambda–5x (black circle) DNA molecules as a function of the inverse average electric field.

Consequently, we experimentally define the mobility as

$$\mu = \frac{L}{TE_{av}} \frac{(1+\gamma)^2}{4\gamma}. \tag{5}$$

The inclusion of the term involving γ results from measuring the mobility as a function of the *average* electric field and means that the expression reduces to the free solution mobility in the limit that the trapping time is negligible. Note that we have written Eq. (3) assuming the DNA is a point particle. The uncertainty in the mobility for a given trial is propagated from the standard deviation of the arrival time as $\delta\mu = \mu \cdot \delta T/T$. By combining Eqs. (2) and (3), we can derive an expression for the average trapping time at a given E_{av} as

$$\tau = \frac{L}{E_{av}} \frac{(1+\gamma)^2}{4\gamma} \left(\frac{1}{\mu} - \frac{1}{\mu_0}\right). \tag{6}$$

Thus, we can determine the average trapping time as a function of E_{av} if we know the free solution mobility. The free solution mobility can be extracted from Eq. (5) at large E_{av} (typically at 40 V/cm) where the trapping time is negligible. We can combine Eqs. (1)–(3) to write the measured mobility as a function of E_{av} as

$$\mu(E_{av}) = \frac{\mu_0}{1 + AE_{av} \exp(B/E_{av}kT)}, \tag{7}$$

TABLE I. Experimental conditions for the mobility measurements including type of DNA, ionic strength of the buffer, fluorescent dye molecule to DNA base pair ratio, and the percentage of PVP solute used to reduce electroosmotic flow.

DNA type	Ionic strength (mM)	Fluorescent ratio (bp:dye)	Electroosmotic suppressor (PVP)	Label
T4	160	5:1	None	T4–5x
T4	95	5:1	None	T4–3x
T4	160	20:1	None	T4–20:1
T4	160	5:1	2%	T4–PVP
Lambda	160	5:1	None	Lambda–5x

where A and B are constants. Note this expression is only physically reasonable for $1/E_{av} \geq kT/B$.

It is expected that the standard deviation of the mobility for a particular experiment depends primarily on the trapping time probability distribution and the number of traps through which the DNA travel, which is proportional to L. For the typical radius of gyration of DNA used in these experiments relative to the deep and shallow slit heights, diffusion from a deep to shallow region is extremely unlikely. Since the trapping time changes significantly as a function of E_{av}, we typically used smaller L for lower values of E_{av}. This makes a comparison of $\delta\mu$ for different E_{av} values non-trivial.

As will be explained in more detail, we observed larger fluctuations in the mobility under fixed conditions than were expected based on statistical fluctuations. Consequently, we measured the DNA mobility under a variety of different conditions, as described in Table I, to determine if these fluctuations correlated with controllable experimental variables. We compare the fluctuations from the different conditions to the nominal condition that we define to be T4 DNA in the 160 mM ionic strength solution with a fluorescent staining ratio of 5:1, which we denote T4–5x. The label for each experimental condition is displayed in Table I and is intended to highlight the main difference between a given condition and the nominal one.

III. RESULTS AND DISCUSSION

A. Mobility measurements

We measured the mobility of T4 and lambda DNA in a 160 mM ionic strength buffer at a fluorescent staining ratio of 5:1, termed experiments T4–5x, and Lambda–5x, respectively. The measured mobility for each of three or four trials at a given value of E_{av} is shown for T4–5x in Fig. 2(b). The error bars on each mobility measurement represent the uncertainty propagated from the standard deviation of the arrival time δT, as seen in Fig. 2(a). In Fig. 2(c), we plot the average of the mobility values at each E_{av} for T4–5x and Lambda–5x with the error bars representing the standard error of the mean. In Fig. 2(d), we plot the trapping lifetime on a logarithmic scale for T4–5x and Lambda–5x as a function of $1/E_{av}$ as determined by Eq. (6), with the free solution mobility obtained from the mobility at $E_{av} = 40\,\mathrm{V/cm}$ for each DNA type, respectively. Movies of T4 DNA molecules traversing the entropic traps in these experiments at average electric fields of 17 and 40 V/cm, respectively, can be found in Figs. S1 and S2 of the supplementary material.[18]

Several interesting features are observed in the plots of Fig. 2. First, we observe a nonlinear relationship between the mobility and E_{av} as well as the entropic trapping phenomenon, whereby longer molecules have a larger mobility. It is clear that the mobility and trapping time of T4 are, respectively, larger and smaller than for lambda at all values of E_{av}. These findings are in qualitative agreement with the results of Han and Craighead.[5] The critical value of the electric field below which molecules are indefinitely trapped is approximately a factor of two larger in our device compared to the data in Fig. 5(b) of Han and Craighead.[5] However, this value clearly depends on γ, which is a factor of 3 larger in our device. The trapping lifetimes in each experiment are similar after accounting for the disparity in the threshold electric field

value. We also observe a hitch in the slope of the trapping time in Fig. 2(d) for each DNA type, with a more pronounced jump for the larger T4 DNA. A similar change in the slope of the trapping time was observed in a simulation (see Fig. 12 of Ref. 8) and in the expected mobility (see Fig. 5 of Ref. 9) and attributed to the role of the electric field deformation at the entrance to the shallow region. Our data is not sufficient to support this hypothesis though it is suggestive.

The mobility at large electric field where the trapping time is estimated as less than 1% of the travel time is approximately $1.4 \times 10^{-4}\,\mathrm{cm}^2/\mathrm{Vs}$ and $1.2 \times 10^{-4}\,\mathrm{cm}^2/\mathrm{Vs}$ for T4 and lambda DNA, respectively. The difference is perhaps surprising since it is known that the free solution mobility of DNA is length independent above a cutoff of approximately 0.4 kbp.[19] We have found that the mobility of T4 and lambda DNA measured in similar depths using fused silica devices made similarly to those here are consistent within their uncertainty at a few percent. Han and Craighead also observed a length based mobility difference at a large electric field[6] and the same finding was reported in a simulation.[8] Presumably this difference in the asymptotic free solution mobility between T4 and lambda in the entropic trapping device is due to differences in relaxation times or effects where the DNA molecules are stretched across multiple traps simultaneously. The problem is rather complicated as the relaxation times are depth dependent.[20] An additional factor might be that the T4 is still slightly compressed in the deep region since its radius of gyration, assumed to be about $(165.6/48.5)^{0.6} = 2.1$ times larger than the ≈700 nm radius of gyration of lambda, is comparable to the depth in that region. Additionally, recent work has shown that DNA molecules are compressed in high electric fields, which may be relevant in the shallow regions.[21]

We can make rough estimations to determine whether the measured mobility values at high electric field are reasonable. A typical value given for the mobility of double stranded DNA in microfluidic devices[1] is within a factor of two of our measurements, though care must be taken to account for the buffer ionic strength and effect of electroosmotic flow. The free solution mobility of DNA in bulk has been measured by Stellwagen *et al.*[19] in a 0.5× TBE buffer (ionic strength of approximately 15 mM) to be $4.5 \times 10^{-4}\,\mathrm{cm}^2/\mathrm{Vs}$. As previously mentioned, the velocity of a DNA molecule at a given electric field strength results from the electric force acting on the DNA and from its frictional drag with the solution. The frictional drag can result both from a bulk flow of the solution and from a local flow generated by hydrodynamic interactions with oppositely charged ions located within about a Debye length. These are both termed electroosmotic though the former results from the surface charge of the silica boundary and the latter from the surface charge of a DNA molecule.

To compare the mobility we measure at large electric field to the value from Stellwagen *et al.*[19] we must account for the electroosmotic flow in the channel (bulk) due to the negatively charged fused silica surface and for the local electroosmotic flow due to counter-ions within about a Debye length of each DNA molecule. For the former, we first estimate the zeta potential ζ of fused silica,[22] the potential approximately at the surface of the fluid boundary, as $\zeta \approx \log_{10}(c) \cdot [2 + 7 \cdot (\mathrm{pH} - 3)]$, where c is the counter-ion concentration in molar units and ζ is in mV. This leads to $\zeta \approx -30\,\mathrm{mV}$ for the given experimental conditions. We can then estimate the electroosmotic mobility of the solution outside of a Debye length from the channel boundary as $\mu_{eos} = -\varepsilon\zeta/\eta = 1.8 \times 10^{-4}\,\mathrm{cm}^2/\mathrm{Vs}$, where ε is the permittivity and η is the viscosity of the buffer. Since the electroosmotic flow reduces the measured DNA mobility from its free solution value, the inferred free solution mobility of DNA in the entropic trap device is about $3.2 \times 10^{-4}\,\mathrm{cm}^2/\mathrm{Vs}$. The estimate of ζ agrees with the surface charge extrapolated from ionic current measurements in fused silica nanofluidic devices,[23] derived using the Grahame equation[24] to relate ζ to the surface charge. This order of magnitude estimate of the electroosmotic flow does not account for the entropic array geometry. We will return to this point in Sec. III C.

We must also account for the reduced local electroosmotic flow around a DNA molecule in our higher ionic strength buffer. Manning[25] has shown that the leading order effect of local drag from oppositely charged ions on the DNA mobility is proportional to $|\ln\kappa b|$, where κ is the inverse Debye length and b is the 0.17 nm distance between negative charges along a DNA

molecule. The free solution mobility expected in a 160 mM solution should then be approximately 55% of the mobility measured in a 15 mM solution.[19] The observed value corrected for the bulk electroosmotic flow then seems reasonable compared to the extrapolated expectation.

However, it is also evident from Fig. 2(b) that the scatter of the individual mobility measurements at a given value of E_{av} is larger than one would expect based on the uncertainty of each measurement. At some values of E_{av}, we observed ~50% variations in the mobility between measurements when each individual measurement had a ~10% fractional uncertainty. Qualitatively, the fractional uncertainty in the average mobility is larger for smaller values of E_{av}, where trapping plays a dominant role relative to drift, as expected. A plot of the average fractional uncertainty of the mobility as a function of E_{av} is shown in Fig. S4 of the supplementary material.[18] Quantitative comparisons as a function of E_{av} are not trivial because we used different separation lengths (different number of traps) for many values of E_{av}. When performing trials of experiments at a new value of E_{av} we were unable to accurately determine the average value until several trials had been completed. While the results demonstrate the validity of the entropic trapping mechanism, it also appears by eye that the monotonic reduction in the mobility for T4 and lambda as E_{av} decreases is not entirely smooth. Since we are motivated to extend the study of entropic trapping to more complicated mechanisms, including ratchet separations and single molecule measurements of conformational changes at the trapping barrier, we investigated the non-statistical variations in the mobility in greater detail.

We attempted to correlate the non-statistical mobility variations with several tunable experimental variables. We first verified that we were using a well-defined protocol for adding buffer to the device, applying electric fields, loading DNA, and performing trials as outlined in Sec. II B. We examined the fluctuations in the mobility as a function of the time between individual trials and were unable to find a reliable correlation. In some cases, mobility measurements were consistent across experiments performed over several consecutive days; in other cases, fluctuations were observed to occur between trials, on a time scale of 1 h. We have not examined whether the fluctuations occur on a shorter time scale. We verified that the ionic current was linear with the applied electric field over the relevant range of E_{av} and that the ionic current was stable within and between measurements to within a few percent using a 95 mM ionic strength buffer with PVP added. However, due to the small volume of fluid contained within a device, we were unable to verify whether electrochemical or other reactions altered the characteristics of the buffer throughout the course of experiments.

We studied the effects of DNA concentration, ionic buffer concentration (T4–3x), adding a polymer to suppress electroosmotic flow (T4–PVP), and the fluorescent dye staining ratio (T4–20:1) on the mobility as shown in Fig. 3. In Fig. 3(a), it is observed that the mobility fluctuates by about 50% over the course of twelve chronological experiments conducted with alternating large and small concentrations, or plugs, of DNA. The data for Fig. 3(a) were obtained using 10 kbp DNA in a separate device with a ratio of deep to shallow depths of ~10, and a similar shallow depth to the nominal device described. The fluctuations in mobility were qualitatively similar to those already described. We estimate that the small and large plugs contain 0.15 and 1.0 nM of molecules, respectively. The time between successive experiments is approximately thirty minutes. The variation appears systematic in time but uncorrelated with the plug concentration. This range of concentrations is about a factor of 5 lower than the overlap concentration[26] for 10 kbp DNA where single molecules begin to interact. It has been observed that the mobility of DNA has about a 10% dependence on the concentration[6] in entropic traps and a larger dependence in gels for concentrations greater than the overlap value.[27] While the mobility steadily increases over the course of experiments shown in Fig. 3(a), this behavior is not necessary repeatable. In some instances, the mobility steadily decreases and in others it oscillates as experiments are repeated.

As shown in Fig. 3(b), the mobility for T4 DNA is about a factor of 2 smaller for the 95 mM compared to the 160 mM ionic strength buffer for intermediate values of E_{av}, and about a factor of 70% smaller at high values of E_{av}. As already explained, there are two predominant competing effects from the reduction in the ionic strength on DNA mobility within these experimental conditions: reduced local drag on a DNA molecule from nearby positively charged

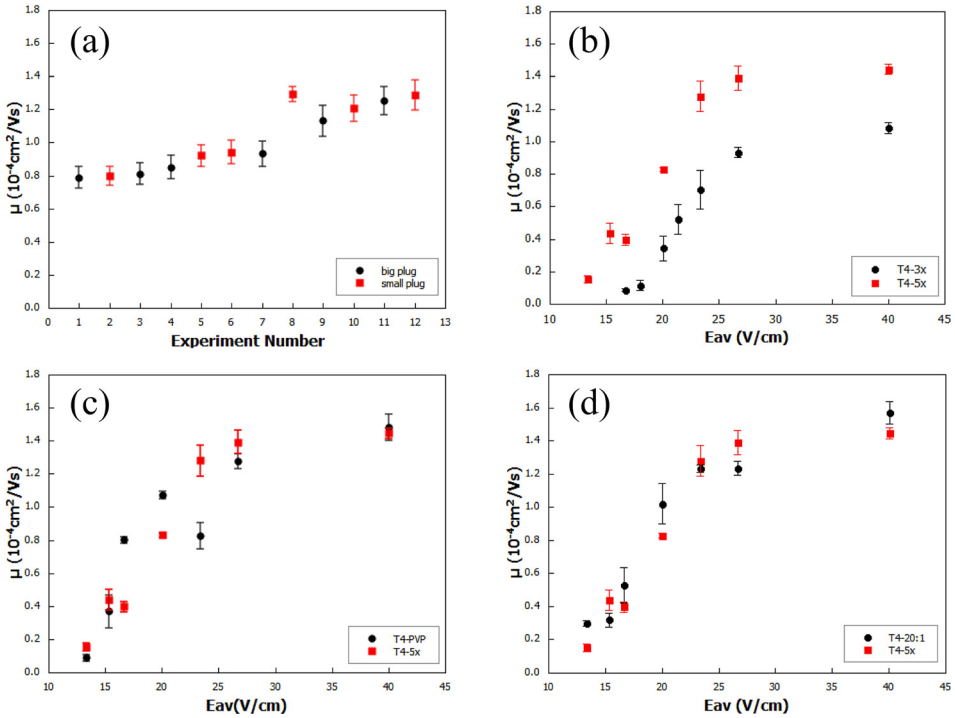

FIG. 3. Comparison of DNA mobility under different experimental conditions as denoted in Table I. Mobility of (a) 10 kbp DNA for large (black circle) and small (red square) DNA loading concentrations in chronological experiments at an average electric field of 26 V/cm; (b) T4–5x (red square) and T4–3x (black circle) to investigate the effect of ionic strengths; (c) T4–5x (red square) and T4–PVP (black circle) to investigate the effect of suppressing electroosmotic flow; and (e) T4–5x (red square) and T4–20:1 DNA to investigate the effect of the fluorescent dye. Note that the mobility measurements in (a) were taken in a separately fabricated device with $\gamma \approx 10$.

counter-ions, and increased bulk electroosmotic flow due to the larger absolute value of the zeta potential. We estimate that the reduction in ionic strength should cause the bulk electroosmotic flow to increase by 40% and the local DNA mobility to increase by about 15%. This leads overall to an expected decrease of the mobility at the lower salt concentration by a factor of 60%. We ignore any effects from changes in the conformation of the DNA due to small variations in the DNA persistence length and width at these ionic strengths.[28] The observed reduction in the mobility at large E_{av} is roughly consistent with our expectation given the nature of the estimation. It is not obvious why the ratio of mobility should vary with E_{av}, as observed in Fig. 3(b), though, with large uncertainty.

The mobility fluctuations appear to be enhanced by the addition of the electroosmotic suppressor PVP as shown in Fig. 3(c). It has been experimentally verified that the addition of low molecular weight PVP reduces electroosmotic flow[29] by binding to fused silica. The physical mechanism for the reduction purportedly results from the PVP either decreasing the absolute value of the zeta potential or increasing the viscosity within a Debye length from the silica boundary or a combination thereof.[30] The addition of PVP to nanoslits with depth on the order of 20 nm has been correlated[31,32] with modulated DNA mobility (high molecular weight PVP is used as sieving medium for this purpose[33]). For some values of E_{av}, the T4–PVP DNA mobility is larger than the T4–5x mobility and for other values it is lower. We expect that reducing the electroosmotic flow would result in higher mobility for T4–PVP for all values of E_{av}. It is not clear whether the increased fluctuations mask this behavior. Note again that the data points represent the mean of four trials at a given value of E_{av}, with the error bar representing the standard error of the mean.

There does not appear to be a significant difference between the mobility of the T4–5x and T4–20:1 samples. There is ongoing discussion in the literature as to the effect that intercalating

dyes have on the physical properties of DNA when bound.[34] The dye has been shown to increase the contour length by 20%–30% at a saturated staining ratio[35] but there are conflicting results concerning its effect on the DNA persistence length. We did not expect to see a significant difference in the average mobility at a given E_{av} from changing the staining ratio. The dye has a low equilibrium binding constant for DNA but will also bind preferentially to fused silica. We wondered whether repeated experiments using DNA stained at the 5:1 ratio led to an increasing amount of dye adsorbing onto the fused silica over time, modulating the zeta potential and the electroosmotic flow. It is not clear why this would have resulted in the bipolar mobility fluctuations we observed but it seemed plausible that a reduced concentration of dye might influence the fluctuations. However, the fluctuations appear qualitatively similar in both samples. The individual mobility measurements for each trial and all experimental conditions can be seen in Fig. S3 of the supplementary material.[18]

B. Mobility fluctuations

To quantify the fluctuations, we perform a non-linear least squares fit to the observed mobility using Eq. (7), with A and B as free parameters as shown in Fig. 4(a). In the fits, the free solution mobility is fixed to the mobility observed at the largest value of E_{av}. Using the results of the fit, we can then calculate a test statistic χ that is the difference between the measured mobility and the mobility given by the fit, divided by the mobility uncertainty. The test statistic is calculated for every trial, not just for the average. However, for the mobility uncertainty we used the average of $\delta\mu$ over the trials at a given value of E_{av}. We write the statistic as $\chi = [\mu_i - f(E_{av})]/\delta\mu_{av}$. We expect that the distribution of χ should be normally distributed with a mean of zero and a width of one if the mobility fluctuations are stochastic in nature. It should be noted that the fits are not particularly robust; there is often a large correlation between the A and B parameters. However, as seen in Fig. 4(a), the fitted function does a reasonable job of passing through the data and is thus acceptable for use in the determination of χ. We do not attempt to draw physical conclusions based on the fitted value of the parameters.

We made histograms of χ for each of the experimental conditions listed in Table I to quantify the mobility fluctuations, as shown in Fig. 4(b) through 4(e). For a given experiment, the sample mean and standard deviation of χ is similar to that returned by a maximum likelihood fit of the histogram to a Gaussian function. A plot of the mean and standard deviation of χ for

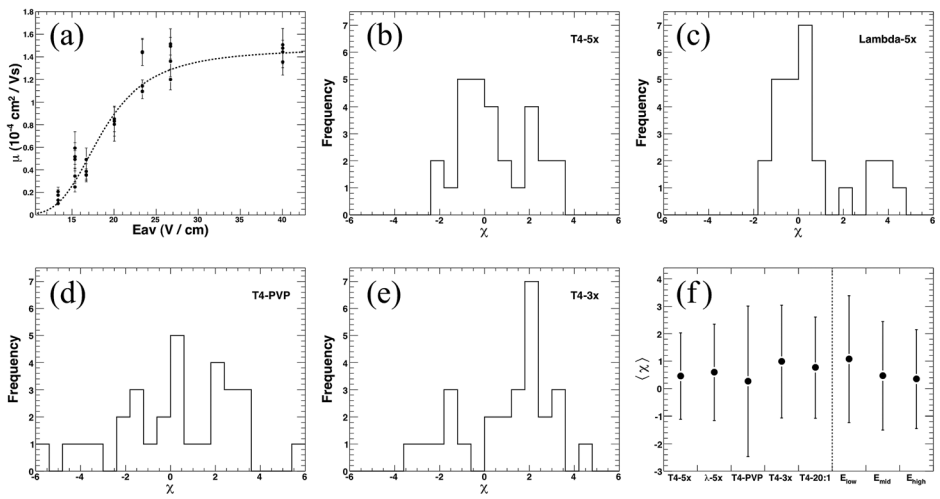

FIG. 4. (a) Mobility for all trials of T4–5x as a function of E_{av}, with the uncertainty for each trial propagated from δT. The dashed line shows the results of the mobility fit to Eq. (7). Histograms of χ, the difference between the measured and fitted mobility of a trial divided by the average uncertainty in the mobility, for the experimental conditions (b) T4–5x, (c) Lambda–5x, (d) T4–PVP, and (e) T4–3x. A summary of the mean and standard deviation (represented by the error bar) of the χ histograms for the labeled experimental conditions, as well as for different values E_{av} when averaged over all the experiments is shown in (f).

each experiment is shown in Fig. 4(f). Additionally, we examined χ at low, middle, and high values of E_{av} integrated over all trials of each experiment. The separating value between the low–middle and middle–high E_{av} regions was arbitrarily chosen by eye to be 16 and 22 V/cm, respectively. This yields two, two, and three data points from each experiment in the low, middle, and high E_{av} regions, respectively. The resulting mean and standard deviations are also show in Fig. 4(f). There is a small positive bias in the mean of χ for all experiments, though it is only significant at the one or two sigma level for any individual experiment. The standard deviations are all significantly larger than one, indicating that the fluctuations are larger than expected based on the uncertainty in the mobility measured from each trial. The experiments with the largest standard deviations are T4–3x and T4–PVP. The fluctuations are also largest at low values of E_{av}, though this may be partially artificial since $f(E_{av})$ is constrained to match the data at high values of E_{av} for each experiment.

C. Discussion

We considered whether the mobility variation could be related to the fabrication process. In an earlier generation of an entropic trap device, we observed that the DNA were not distributed uniformly across the separation channel width, but were preferentially moving along a particular side. The deep and shallow sections of the earlier device were designed to have the same widths. However during the alignment process, the deep regions were misaligned by approximately 2 μm relative to the already etched shallow regions. We speculated that the misalignment was responsible for the DNA preferring to align along the side of the channel where the shallow region's width extended beyond that of the deep region, though we did not have a physical model to explain this observation. As stated in Sec. II A, for the device described herein, the width of the deep region was designed to be wider than the shallow region to avoid edge effects due to misalignment. After this correction to the device design, we observed that the DNA molecules were uniformly distributed along the width of the separation channel at the observation region as expected. We have also measured the mobility of DNA in devices containing a single long deep and shallow region (similar to the devices used in previous measurements[36]). The mobility values measured in these devices were consistent within a few percent over several days of measurements.

We note that Thomas *et al.*[17] have also observed a non-statistical variation in the mobility of short DNA molecules (order several hundred base pairs) that occurred over hours in similar entropic trap devices. These devices were made from fluidic channels etched in silicon and anodically bonded to fused silica cover slips. The magnitude of the mobility variations observed between identical measurements in these experiments was also on the order of 50% or larger. Variations in DNA mobility on the order of 15% for identical experiments run on consecutive days have similarly been observed in microfluidic devices containing an array of posts.[37] The physical mechanism of DNA separation in the devices of Thomas *et al.*[17] is distinct from that studied here since the DNA molecules they used did not have to deform to pass from a deep to shallow region in their devices. The separation process is more analogous to size exclusion chromatography. The observation of mobility variation by another experimental group using a separate fabrication method, substrate material, and DNA molecular length lends credibility to the conjecture that the mobility variation is not specific to our particular methods. Instead it may be an intermittent feature of nanofluidic DNA separations in complicated geometries. This must be partially contrasted, however, with the results of Han and Craighead[7] that indicated only approximately 10% variation in the asymptotic mobility at large values of E_{av} over month timescales. It is still possible then that the fluctuations are enhanced at lower values of E_{av} when the trapping time is significant as observed here.

The effect of a non-uniform bulk electroosmotic flow in capillary electrophoresis due to changes in the channel geometry, the zeta potential, or both have been well studied.[38–42] It has been shown in varying limits that such changes can give rise to circulating electroosmotic flows and lead to unwanted axial dispersion in electrophoretic separations.[43] A general review of these results can be found in Ref. 44. In our device, the decrease in channel height of more

than 1 μm over an axial distance of around 1 μm does not lend itself to an easy solution for the flow. Additionally, the simplification afforded by the Debye-Huckel linearization when $\zeta e \ll kT$ is questionable using fused silica at physiological pH values, where e is the electron charge. We performed several additional trials where we optically observed the motion of DNA molecules as they traversed several periods of traps at different regions along the separation channel. We never detected circulatory flow or rapid changes in the DNA mobility. We have observed transient circulatory motion of similarly sized DNA molecules in unpublished work near constrictions in sub-micron fluidic channels. This has led us to consider whether the fluctuations may be due to concentration polarization effects at the deep and shallow interface or nonlinear electrokinetic flow.[45,46] Santiago and co-workers[47,48] have analytically and experimentally determined a boundary in a two-dimensional parameter space that determines whether concentration polarization regions expand throughout the channel in what they refer to as shock waves. For the experiments we have described (with a relatively high salt concentration), the values of these parameters place us far into the regime where the polarization regions do not propagate.

To briefly summarize the main results, we observed mobility fluctuations that were increased in a reduced ionic strength buffer and when a polymer was added at low volume fraction to reduce the electroosmotic flow. The fluctuations were more prevalent at lower values of E_{av} where the trapping time was dominant. The fluctuations occurred between experiments that were roughly thirty minutes apart, though we cannot rule out that they occur on a shorter time scale as well. We do not believe that the fluctuations result from any particular method of the fabrication process or the substrate material. We surmise that the fluctuations may be due to changes in the zeta potential and the corresponding electroosmotic flow when buffer ions, fluorescent dye, or DNA molecules adsorb to the fused silica surface during an experiment. This adsorption might be enhanced by the channel geometry. The measured ionic current is not sensitive to these changes at the salt concentrations used within the experimental resolution. It is still not obvious given this explanation why the fluctuations would sometimes increase and sometimes decrease the mobility from experiment to experiment. In future work we hope to investigate the electroosmotic flow in various ionic strength buffers in more detail. We are planning experiments to use a caged-fluorescence imaging technique[49] that should allow us to optically obtain information about the fluid flow near the interface between the deep and shallow regions. We also intend to implement a continuous tracking system with time-lapse capabilities to track the DNA plug as it traverses the entropic trap array. It is important to note that microfluidic devices are typically used to separate many different sized molecules simultaneously with a molecule of known length included as a standard reference. The variations that we observed are inconsequential when measuring the relative mobility of an unknown molecular length to a standard, which is common practice when using microfabricated devices[6] or gels for DNA separation.

IV. CONCLUSIONS

We measured the mobility of T4 and Lambda DNA molecules in nanofluidic entropic traps under a variety of experimental conditions. We found that longer DNA molecules had a larger mobility and that the mobility depended nonlinearly on the electric field in agreement with previous research. We observed fluctuations in the mobility from trial to trial that were larger than expected based on the statistical uncertainty of the mobility in any given trial. These fluctuations were moderately enhanced at lower values of the electric field when the trapping time was significant relative to the electric field induced drift time for a period of the trap. The fluctuations were also moderately larger when an electroosmotic-suppressing polymer was added and in a reduced ionic strength buffer.

ACKNOWLEDGMENTS

This work was performed in part at the Binghamton University Nanofabrication Facility and at the Cornell NanoScale Facility, a member of the National Nanotechnology Infrastructure Network,

which is supported by the National Science Foundation (Grant No. ECCS-0335765). This research was supported by NSF Grant No. DMR-1351283. We thank Professor S. Ghosal and an anonymous reviewer for their helpful comments.

[1]K. D. Dorfman, "DNA electrophoresis in microfabricated devices," Rev. Mod. Phys. **82**, 2903 (2010).
[2]S. L. Levy and H. G. Craighead, "DNA manipulation, sorting, and mapping in nanofluidic systems," Chem. Soc. Rev. **39**, 1133–1152 (2010).
[3]R. B. Schoch, J. Han, and P. Renaud, "Transport phenomena in nanofluidics," Rev. Mod. Phys. **80**, 839 (2008).
[4]J. Han and H. G. Craighead, "Entropic trapping and sieving of long DNA molecules in a nanofluidic channel," J. Vac. Sci. Technol., A **17**, 2142 (1999).
[5]J. Han, S. W. Turner, and H. G. Craighead, "Entropic trapping and escape of long DNA molecules at submicron size constriction," Phys. Rev. Lett. **83**, 1688–1691 (1999).
[6]J. Han and H. G. Craighead, "Separation of long DNA molecules in a microfabricated entropic trap array," Science **288**, 1026 (2000).
[7]J. Han and H. G. Craighead, "Characterization and optimization of an entropic trap for DNA separation," Anal. Chem. **74**, 394–401 (2002).
[8]F. Tessier, J. Labrie, and G. W. Slater, "Electrophoretic separation of long polyelectrolytes in submolecular-size constrictions: A Monte Carlo study," Macromolecules **35**, 4791–4800 (2002).
[9]T. Sakaue, "DNA electrophoresis in designed channels," Eur. Phys. J. E: Soft Matter Biol. Phys. **19**, 477–487 (2006).
[10]A. S. Panwar and S. Kumar, "Time scales in polymer electrophoresis through narrow constrictions: A Brownian dynamics study," Macromolecules **39**, 1279–1289 (2006).
[11]K. L. Sebastian and A. K. R. Paul, "Kramers problem for a polymer in a double well," Phys. Rev. E **62**, 927–939 (2000).
[12]C. T. A. Wong and M. Muthukumar, "Scaling theory of polymer translocation into confined regions," Biophys. J. **95**, 3619–3627 (2008).
[13]Z. Chen and A. Fernando, "Escobedo simulation of chain-length partitioning in a microfabricated channel via entropic trapping," Mol. Simul. **29**, 417–425 (2003).
[14]Y. M. Lee and Y. L. Joo, "Brownian dynamics simulations of polyelectrolyte molecules traveling through an entropic trap array during electrophoresis," J. Chem. Phys. **127**, 124902 (2007).
[15]M. Streek, F. Schmid, T. T. Duong, and A. Ros, "Mechanisms of DNA separation in entropic trap arrays: A Brownian dynamics simulation," J. Biotechnol. **112**, 79–89 (2004).
[16]F. Tessier and G. W. Slater, "Strategies for the separation of polyelectrolytes based on non-linear dynamics and entropic ratchets in a simple microfluidic device," Appl. Phys. A: Mater. Sci. Process. **75**, 285–291 (2002).
[17]J. D. P. Thomas, M. N. Joswiak, D. W. Olson, S.-G. Park, and K. D. Dorfman, "Ratchet nanofiltration of DNA," Lab Chip **13**, 3741–3746 (2013).
[18]See supplementary material at http://dx.doi.org/10.1063/1.4887395 for movies of T4 DNA traversing the entropic traps and additional plots.
[19]N. C. Stellwagen, C. Gelfi, and P. G. Righetti, "The free solution mobility of DNA," Biopolymers **42**, 687–703 (1997).
[20]J. Tang, S. L. Levy, D. W. Trahan, J. J. Jones, H. G. Craighead, and P. S. Doyle, "Revisiting the conformation and dynamics of DNA in slitlike confinement," Macromolecules **43**, 7368–7377 (2010).
[21]J. Tang, N. Du, and P. S. Doyle, "Compression and self-entanglement of single DNA molecules under uniform electric field," Proc. Natl. Acad. Sci. U.S.A. **108**, 16153–16158 (2011).
[22]B. J. Kirby and E. F. Hasselbrink, "Zeta potential of microfluidic substrates: 2. Data for polymers," Electrophoresis **25**, 203–213 (2004).
[23]D. Stein, M. Kruithof, and C. Dekker, "Surface-charge-governed ion transport in nanofluidic channels," Phys. Rev. Lett. **93**, 035901 (2004).
[24]J. N. Israelachvili, *Intermolecular and Surface Forces*, 3rd ed. (Academic Press, 2011).
[25]G. S. Manning, "Limiting laws and counterion condensation in polyelectrolyte solutions. 7. Electrophoretic mobility and conductance," J. Chem. Phys. **85**, 1506–1515 (1981).
[26]M. Rubinstein and R. H. Colby, *Polymer Physics* (OUP, Oxford, 2003).
[27]N. Pernodet and B. Tinland, "Influence of λ-DNA concentration on mobilities and dispersion coefficients during agarose gel electrophoresis," Biopolymers **42**, 471–478 (1997).
[28]C. C. Hsieh, A. Balducci, and P. S. Doyle, "Ionic effects on the equilibrium dynamics of DNA confined in nanoslits," Nano Lett. **8**, 1683–1688 (2008).
[29]T. Kaneta, T. Ueda, K. Hata, and T. Imasaka, "Suppression of electroosmotic flow and its application to determination of electrophoretic mobilities in a poly(vinylpyrrolidone)-coated capillary," J. Chromatogr. A **1106**, 52–55 (2006).
[30]G. W. Slater, F. Tessier, and K. Kopecka, "The electroosmotic flow (EOF)," in *Microengineering in Biotechnology* (Humana Press, 2010), pp. 121–134.
[31]J. D. Cross, E. A. Strychalski, and H. G. Craighead, "Size-dependent DNA mobility in nanochannels," J. Appl. Phys. **102**, 024701 (2007).
[32]O. Castillo-Fernandez, G. B. Salieb-Beugelaar, J. W. van Nieuwkasteele, J. G. Bomer, M. Arundell, J. Samitier, A. van den Berg, and J. C. T. Eijkel, "Electrokinetic DNA transport in 20 nm-high nanoslits: Evidence for movement through a wall-adsorbed," Electrophoresis **32**, 2402–2409 (2011).
[33]Q. Gao and E. S. Yeung, "A matrix for DNA separation: Genotyping and sequencing using poly(vinylpyrrolidone) solution in uncoated capillaries," Anal. Chem. **70**, 1382–1388 (1998).
[34]D. R. Tree, A. Muralidhar, P. S. Doyle, and K. D. Dorfman, "Is DNA a good model polymer?," Macromolecules **46**, 8369–8382 (2013).
[35]O. B. Bakajin, T. A. J. Duke, C. F. Chou, S. S. Chan, R. H. Austin, and E. C. Cox, "Electrohydrodynamic stretching of DNA in confined environments," Phys. Rev. Lett. **80**, 2737–2740 (1998).
[36]E. A. Strychalski, S. L. Levy, and H. G. Craighead, "Diffusion of DNA in nanoslits," Macromolecules **41**, 7716–7721 (2008).

[37]J. Ou, S. J. Carpenter, and K. D. Dorfman, "Onset of channeling during DNA electrophoresis in a sparse ordered post array," Biomicrofluidics **4**, 013203 (2010).
[38]J. L. Anderson and W. K. Idol, "Electroosmosis through pores with nonuniformly charged walls," Chem. Eng. Commun. **38**, 93–106 (1985).
[39]A. Ajdari, "Electro-osmosis on inhomogeneously charged surfaces," Phys. Rev. Lett. **75**, 755–758 (1995).
[40]D. Long, H. A. Stone, and A. Ajdari, "Electroosmotic flows created by surface defects in capillary electrophoresis," J. Colloid Interface Sci. **212**, 338–349 (1999).
[41]S. Ghosal, "Effect of analyte adsorption on the electroosmotic flow in microfluidic channels," Anal. Chem. **74**, 771–775 (2002).
[42]S. Ghosal, "Lubrication theory for electro-osmotic flow in a microfluidic channel of slowly varying cross-section and wall charge," J. Fluid Mech. **459**, 103–128 (2002).
[43]S. Ghosal, "The effect of wall interactions in capillary-zone electrophoresis," J. Fluid Mech. **491**, 285–300 (2003).
[44]S. Ghosal, "Electrokinetic flow and dispersion in capillary electrophoresis," Annu. Rev. Fluid Mech. **38**, 309–338 (2006).
[45]T. A. Zangle, A. Mani, and J. G. Santiago, "Theory and experiments of concentration polarization and ion focusing at microchannel and nanochannel interfaces," Chem. Soc. Rev. **39**, 1014–1035 (2010).
[46]S. J. Kim, Y.-A. Song, and J. Han, "Nanofluidic concentration devices for biomolecules utilizing ion concentration polarization: theory, fabrication, and applications," Chem. Soc. Rev. **39**, 912 (2010).
[47]A. Mani, T. A. Zangle, and J. G. Santiago, "On the propagation of concentration polarization from microchannel−nanochannel interfaces Part I: Analytical model and characteristic analysis," Langmuir **25**, 3898–3908 (2009).
[48]T. A. Zangle, A. Mani, and J. G. Santiago, "On the propagation of concentration polarization from microchannel−nanochannel interfaces Part II: Numerical and experimental study," Langmuir **25**, 3909–3916 (2009).
[49]A. E. Herr, J. L. Molho, J. G. Santiago, M. G. Mungal, T. W. Kenny, and M. G. Garguilo, "Electroosmotic capillary flow with nonuniform zeta potential," Anal. Chem. **72**, 1053–1057 (2000).